Available online at www.sciencedirect.com
SCIENCE DIRECT®
Chemical Physics 305 (2004) 13–26
Chemical Physics
www.elsevier.com/locate/chemphys

A DFT study of asymmetric *meso*-substituted porphyrins and their zinc complexes

Oana Cramariuc [a,b,*], Terttu I. Hukka [b], Tapio T. Rantala [a]

[a] *Department of Chemistry, Institute of Physics, Tampere University of Technology, Korkeakoulunkatu 8, Festia, P.O. Box 692, FIN-33101 Tampere, Finland*
[b] *Institute of Materials Chemistry, Tampere University of Technology, P.O. Box 541, FIN-33101 Tampere, Finland*

Received 8 March 2004; accepted 4 June 2004
Available online 10 July 2004

Abstract

In the present work density functional theory (DFT) is applied to calculate geometries and electronic structures of 3,4-dimethyl-*N*-{2-[10,15,20-tris-(3,5-di-*tert*-butyl-phenyl)-porphyrin-5-yl]-phenyl}benzamide (H_2P–O34) and its zinc complex (ZnP–O34). The influences of the substituents in the porphyrin ring on the energies of frontier molecular orbitals are evaluated. This is done by gradually increasing the amount of substituents in the investigated porphine and zinc porphine rings. The DFT framework used in this work is found to correctly describe the differences in electronic structures, which arise from differences in the location, number, and electronic effects of the substituents at the *meso*-positions of the porphyrin ring. In addition, the applicability of the ground state DFT method for evaluating the one-electron transition energies, which correspond to the near UV–Vis optical absorptions of porphyrin molecules, is investigated. The transition energies and the orbitals involved in electronic transitions are well reproduced by this method, as shown by comparing the results to our time dependent density functional calculations.

Keywords: DFT; Porphyrins

1. Introduction

The molecular structures and the electronic properties of porphyrin–fullerene dyads, in which either H_2P–O34 or its zinc porphyrin complex ZnP–O34 acts as an electron donating unit, have been studied by various experimental methods during the past years [1–3]. The experimental results suggest that a photoinduced electron transfer to the acceptor could lead to a formation of a charge-separated state which lives long enough to make it possible to fabricate molecular optoelectronic devices [1].

The type of central metal ion together with the number, locations, and types of substituents attached to a porphyrin ring have been shown both experimentally [4–10] and theoretically [6,11–20] to influence the electronic structures and accordingly, the optical absorption properties of porphyrins [5–7,10–12,15,18] and metalloporphyrins [4,7,10–13,18,20]. Therefore, the structural tailoring should be carefully considered when porphyrins are designed for molecular optoelectronic applications.

The experimental near UV–Vis absorption spectra of porphyrin compounds consist of a very strong absorption band called the Soret band or the B band in the near UV region and of four weak absorptions called the Q band in the visible region. The wavelengths corresponding to the absorption maxima vary depending on the experimental setup [21–23]. In the gas phase spectrum of porphine the absorption maximum of the B band is at 372.0 nm. The peaks of the Q band have been given the labels Q_x^0, Q_x^1, Q_y^0, and Q_y^1 in literature. The Q_x^1 and Q_y^1 are generally interpreted as vibronic transitions and Q_x^0 and Q_y^0 peaks as pure electronic transitions [24,25]. Therefore, the calculated wavelengths should be

* Corresponding author. Tel.: +3580331153635; fax: +358033115 2108.
E-mail addresses: oana.cramariuc@tut.fi (O. Cramariuc), Terttu.Hukka@tut.fi (T.I. Hukka), Tapio.Rantala@tut.fi (T.T. Rantala).

0301-0104/$ - see front matter © 2004 Elsevier B.V. All rights reserved.
doi:10.1016/j.chemphys.2004.06.024

compared to the experimental wavelengths [21] corresponding to the maxima of the Q_x^0 and Q_y^0 peaks, which occur at 627.0 and 511.5 nm in the experimental gas phase spectrum of porphine. The experimental absorption spectra of metalloporphyrins differ from those of porphyrins mainly by having a different number of absorptions in the Q band. There are only two Q band absorptions in metalloporphyrins.

The density functional theory (DFT) with its usual approximations, local density approximation (LDA) and generalized gradient approximation (GGA), is a well established approach for calculating electronic ground states [26–28]. Furthermore, the ground state one-electron picture of DFT has been successfully used to model even excited states after intramolecular transitions between delocalized one-electron orbitals in large organic molecules [29–34] or solids [35–42]. In particular, DFT/B3LYP has also been used to predict the structures and energetics of low-lying triplet states of porphine [20]. The ground state based method becomes attractive for the study of electron transfer processes in dyads because it offers an intuitive picture of various physicochemical characteristics of transitions and excited states, such as energies, charge separation, and geometrical relaxations of metastable states, and even of the influence of the environment [29–34]. Also, it should be noted that in the time dependent DFT (TD-DFT) method, which is formally a rigorous DFT-based method for studying excitation spectra, the differences between the eigenvalues of the ground state Kohn–Sham (KS) orbitals are first approximations to the excitation energies [26].

This paper presents DFT calculations of equilibrium geometries and energies of frontier molecular orbitals (FMOs) of ground states together with one-electron transitions corresponding to the near UV–Vis optical absorptions of H_2P–O34 and ZnP–O34. In addition, isoamplitude surfaces of some FMO wavefunctions have been calculated. The influences of the substituents on the energies of FMOs are analyzed. For this purpose the whole series from porphine and zinc porphine via gradually substituted porphyrins, namely 5,10,15,20-tetraphenyl-porphyrin (TPP), 5,10,15-tris-(3,5-di-*tert*-butyl-phenyl)-20-phenyl-porphyrin (tris-TBPP) and their zinc complexes, Zn–TPP and Zn–tris-TBPP to fully substituted H_2P–O34 and ZnP–O34, have been investigated.

Also the applicability of the ground state based method for studying electronic transitions of porphyrins will be assessed in this work. It will be done by calculating the electronic transitions of porphine using both the DFT and the TD-DFT methods and by comparing the obtained results. The geometries and electronic structures of the ground states along with the symmetries and energies of the excited states of porphine [12,19,43–56] and zinc porphine [14,44,51,57] have been previously investigated by several computational methods. Therefore, porphine and zinc porphine are very good reference compounds for comparing the results obtained within the current DFT framework to those obtained either within the other DFT [14,19,45,46,48,52–54,56,57] frameworks or by other first principles [46,47,49,51] calculations.

2. Computational methods

All DFT calculations have been carried out using the Dmol3 software [58]. The geometry optimizations as well as the subsequent DFT calculations have been performed using the generalized gradient approximation (GGA) and the parameter free Perdew–Wang (PW91) exchange-correlation functional [59] as implemented in this software. Numerically evaluated atomic orbitals as available in the software were used as basis sets. The double-numerical basis set with polarization functions (DNP) includes also ionic orbitals, hydrogenic orbitals, and orbitals of excited states and it consists of three basis functions for H ($1s^1|1s^02p^0$), seven for each C, N, and O ($1s^22s^22p^2|2s^02p^03d^03d^0$), and 10 for Zn ($1s^22s^22p^63s^23p^63d^{10}4s^2|3d^04s^04p^0$).

The energies of one-electron transitions have been calculated as the differences between the energies of unoccupied and occupied one-electron ground state molecular orbitals. Only singlet states have been considered. Transition energies corresponding to the experimentally observed near UV–Vis optical absorptions of porphyrins, i.e., those in the region of 350–750 nm only, have been taken into account. The oscillator strengths (absorption intensities) have been evaluated, as well. The oscillator strengths [60] have been calculated from the transition dipole moments computed within the Dmol3 software.

TD-DFT calculations have been performed using the Turbomole software package [61]. First step of the TD-DFT calculations employs a self-consistent ground state KS computation. The GGA type Perdew–Burke–Ernzerhof (PBE) exchange-correlation functional [59,62–64], as implemented in the Turbomole software package [61], has been used in the calculations. This exchange-correlation functional has been found to yield essentially identical results with PW91 [62,65,66].

Second step consists of solving the central equation of the TD-DFT response theory by using the adiabatic local density approximation (ALDA) for the functional derivatives of the exchange-correlation potential. The Karlsruhe split-valence basis set [67] augmented with polarization functions [68] (SVP) has been used. The SVP basis set consists of two basis functions for H (4s)/[2s], six basis functions for C (7s4p1d)/[7s4p1d], and six basis functions for N (7s4p1d)/[3s2p1d]. The terms in round brackets represent the number of primitive basis

functions of each type and the terms in square brackets represent the number of contracted basis functions of each type. Prior to the TD-DFT calculations, the geometry of porphine was optimized at the DFT/PBE/SVP level. The resolution of the identity approach [69] (RI) has been used to reduce the computational effort and thereby to speed up the calculations.

3. Results

3.1. Porphine

The geometry of porphine optimized with the DNP basis set is illustrated in Fig. 1; labels indicate the α,β, and *meso*-carbons and the pyrrole rings. Table 1 lists some bond lengths and bond angles of porphine calculated with the PW91 functional and the DNP basis set using the Dmol3 software, together with those calculated with the PBE functional and SVP basis set using the Turbomole software. Also the experimental values as well as the values calculated by other groups and methods are provided in Table 1. The results obtained from both DFT calculations are comparable in accuracy with those reported for the calculations performed using hybrid functionals, i.e., DFT/B3LYP/6-31G(d) and DFT/B3LYP/6-31G(df,p)(5d,7f) [19,52,53]. Our calculations yield mean absolute deviations of only 0.004–0.005 Å and of only 0.5–0.6° from the experimental values. These small deviations prove that the computed structure of porphin very closely corresponds to the experimentally observed equilibrium geometry.

The calculated symmetries of some FMOs of porphine are listed in Table 2 along with some results from previous DFT calculations reported in literature. Inspection of Table 2 reveals that there are no essential differences between the symmetries of the lowest unoccupied and highest occupied molecular orbitals calculated by different methods. In addition, the energy differences between the energy of the highest-occupied molecular orbital (HOMO), which has been taken as a reference, and the energies of FMOs are given in Table 2. Both of our DFT calculations yield a gap of approximately 1.95 eV between HOMO and the lowest-unoccupied molecular orbital (LUMO). Same energy gap has been obtained by using a LDA type functional, as reported by Lamoen and Parinello [48]. However, the DFT calculations employing the B3LYP hybrid func-

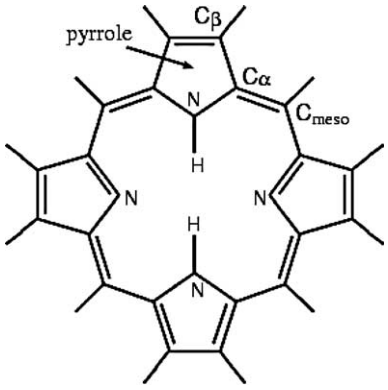

Fig. 1. Optimized molecular structure of porphine.

Table 1
Calculated and experimental bond lengths (Å) and bond angles (°) of porphine

Structural parameters	DFT/PW91/DNP (this work)	DFT/PBE/SVP (this work)	DFT/LDA/ DND [46]	DFT/BLYP/ DNP [45]	DFT/B3LYP/ 6-31G(d) [19,52]	DFT/B3LYP/ 6-31G(df,p)(5d,7f) [53]	Experimental [76]
H–N	1.022	1.031	1.03	1.038	1.015	1.015	
N–C_α	1.375	1.377	1.36	1.365	1.372	1.370	1.367
(N–C_α)[a]	1.367	1.368	1.36	1.363	1.364	1.363	1.364
C_β–C_α	1.435	1.441	1.42	1.423	1.435	1.436	1.438
(C_β–C_α)[a]	1.458	1.466	1.44	1.445	1.460	1.462	1.463
C_β–C_β	1.376	1.382	1.37	1.371	1.372	1.372	1.373
(C_β–C_β)[a]	1.362	1.368	1.35	1.358	1.356	1.356	1.354
C_m–C_α	1.396	1.404	1.38	1.384	1.394	1.394	1.392
(C_m–C_α)[a]	1.402	1.410	1.38	1.390	1.400	1.400	1.393
C_β–H	1.086	1.098	1.09	1.094	1.082	1.080	
(C_β–H)[a]	1.087	1.099	1.09	1.095	1.083	1.082	
C_m–H	1.090	1.101	1.09	1.098	1.086	1.086	
α(H–N–C_α)	124.5	124.6	124.8	125.0	124.6	124.6	
α(C_α–N–C_α)	110.8	110. 8	110.4	110.1	110.9	110.8	109.6
α(C_α–N–C_α)[a]	105.4	105.4	105.0	104.9	105.4	105.5	105.7
α(N–C_α–C_β)	106.6	106.8	107.1	107.2	106.5	106.5	107.8
α(N–C_α–C_β)[a]	111.1	111.3	111.4	111.4	111.1	111.0	110.9
α(C_α–C_β–C_β)	108.0	107.8	107.7	107.7	108.0	108.0	107.4
α(C_α–C_β–C_β)[a]	106.2	106.0	106.1	106.9	106.2	106.2	106.3
α(C_α–C_m–C_α)	127.3	127.1	126.5	126.3	127.1	127.1	127.4

[a] Bonds and angles are in the pyrrole rings in which the nitrogen atoms are unprotonated.

Table 2
Calculated symmetries and energies (ε) of the frontier molecular orbitals of porphine

MO	DFT/PW91/ DNP (this work)		DFT/PBE/ SVP (this work)		DFT/LDA/PZ [49]		DFT/B3LYP/6-31G(df,p)(5d,7f) [53]		DFT/B3LYP/VTZP [54]	
		ε (eV)		ε (eV)		ε (eV)		ε (eV)		ε (eV)
LUMO + 5	b_{3g}	5.47	b_{3g}	5.43					b_{2g}	6.72
LUMO + 4	b_{2g}	5.43	b_{2g}	5.40					a_g	6.48
LUMO + 3	b_{1u}	5.05	b_{1u}	5.02					b_{1u}	6.41
LUMO + 2	a_u	3.28	a_u	3.22	a_u	3.32			a_u	4.46
LUMO + 1	b_{3g}	1.95	b_{2g}	1.92	b_{3g}	1.98	b_{2g}	2.93	b_{2g}	2.88
LUMO	b_{2g}	1.95	b_{3g}	1.91	b_{2g}	1.96	b_{3g}	2.92	b_{3g}	2.87
HOMO	b_{1u}	0	b_{1u}	0	b_{1u}	0	b_{1u}	0	b_{1u}	0
HOMO − 1	a_u	−0.24	a_u	−0.27	a_u	−0.25	a_u	−0.14	a_u	−0.24
HOMO − 2	b_{3g}	−0.82	b_{3g}	−0.86	b_{2g}	−0.81			b_{3g}	−1.18
HOMO − 3	b_{1u}	−0.96	b_{1u}	−0.98	b_{1u}	−0.94			b_{1u}	−1.31
HOMO − 4	a_g	−1.36	b_{2u}	−1.27	a_g	−1.27			b_{2g}	−2.04
HOMO − 5	b_{2u}	−1.36	a_g	−1.29	b_{3u}	−1.29			b_{1u}	−2.09
HOMO reference		−5.17		−4.90		−3.90		−5.16		−5.37

The energies have been calculated with HOMO orbital as a reference.

tional [53,54] yield a larger HOMO–LUMO gap of approximately 3 eV.

The calculated absorption wavelengths, oscillator strengths, and the orbitals involved in the electronic transitions of porphine are presented in Fig. 2 together with the experimental near UV–Vis absorption spectrum [21]. The DFT results are shown in the upper graph (a) and the TD-DFT results in the graph immediately below (b). In the case of the TD-DFT calculations also the one-electron levels which contribute the most to the excitations and the corresponding excitation weights (%) are given in Fig. 2(b). The excitations with excitation weights smaller than 5%, are not shown. The calculated and experimental values are given in Table 3. In addition, the wavelengths corresponding to the electronic transitions computed by the multireference Møller–Plesset perturbation (MRMP) theory [51], DFT-SCI [54], TD-DFT/BP [19,55,56], TD-DFT/PW91 [19,55], and TD-DFT/B3LYP [19,56] methods are presented schematically in Fig. 2(c).

Our TD-DFT calculations yield results, which are similar to those obtained by the TD-DFT calculations employing non-hybrid functionals (BP, PW91). Detailed interpretations of the calculated transitions and comparisons with the experimental data are found in literature [19,55,56], we however, concentrate on the differences between the results obtained with the DFT and TD-DFT methods. Inspection of Fig. 2 and Table 3 reveals that the wavelengths corresponding to the one-electron transitions obtained from the DFT calculations are in a close agreement with those obtained by TD-DFT. Absorptions at 637.3, 566.8 and 346.5 nm each correspond to two overlapping one-electron transitions. Also the transitions at 426.7 and 426.3 nm obtained by the DFT calculations have a counterpart at the TD-DFT level, see Fig. 2 and Table 3. The DFT based approach does not include mixing of the electronic transitions, as does TD-DFT, but almost the same orbitals can be identified as being involved in the transitions. The DFT calculations yield electronic transition wavelengths, which are in a good agreement with the experimental values as well as with the values obtained by the TD-DFT method. However, DFT fails in evaluating the oscillator strengths, see Fig. 2, yielding very low oscillator strengths for the B band and too large oscillator strengths for the Q band. The failure is obviously related to too simple description of the excitations. This drawback of the DFT approach is less important in our ongoing project, which concentrates on tracing the transfer paths of electrons, i.e., the orbitals which are mainly involved in electronic transitions, within porphyrin based donor–acceptor dyads and on predicting the structures and energetics of the corresponding states. Our present DFT and TD-DFT results as well as the DFT results reported in literature [29–34] suggest that DFT can offer in this sense an intuitive and transparent picture of electron transfer processes, in which structures and energies of well-defined final states are calculated.

3.2. Zinc porphine

The geometry of zinc porphine was optimized using the DNP basis set and is illustrated in Fig. 3 together with the wavefunctions of some FMOs, which are presented as isoamplitude surfaces. The complete set of Cartesian coordinates is available on request. The energies of the FMOs have also been calculated and will be discussed below together with the substituted porphyrin molecules.

The wavelengths and the oscillator strengths of the electronic transitions have been calculated using DFT and they are presented together with the experimental absorption spectrum [70] in Fig. 4. The experimental

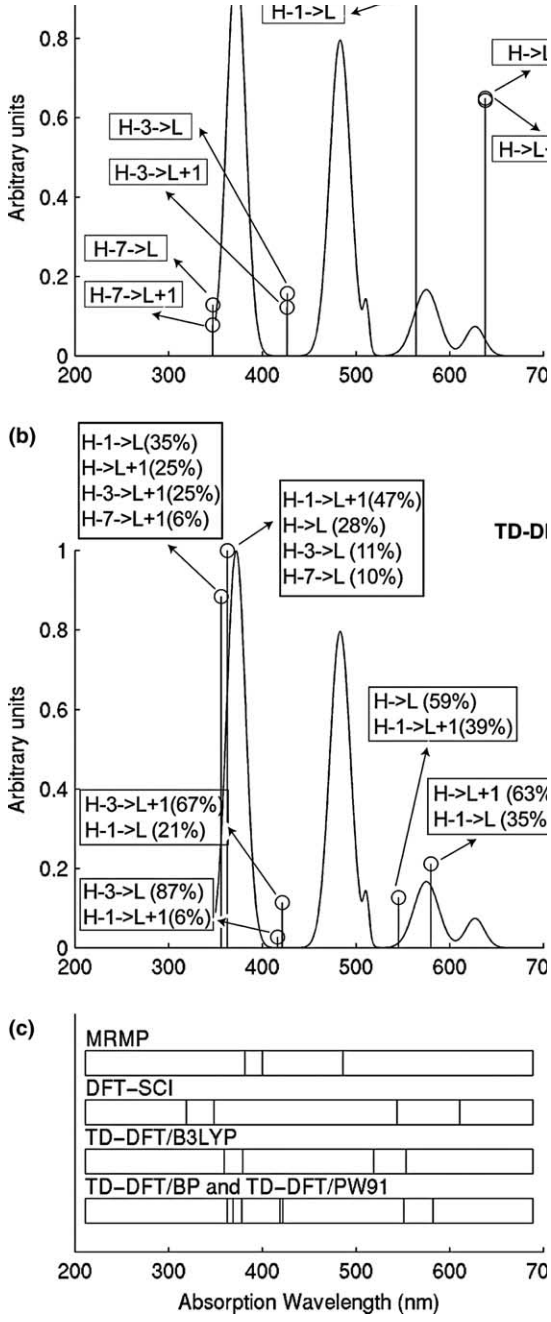

Fig. 2. (a) Electronic transitions of porphine in the region of 350–700 nm. The normalized oscillator strengths calculated by (a) the DFT and (b) the TD-DFT methods are presented as a function of the calculated absorption wavelength (nm) using separate vertical lines. The TD-DFT oscillator strengths at 578.3 and 543.7 nm have been multiplied by 100 prior to normalization. The major contributions from one-electron levels to the excitation energies are given in percents in the case of the TD-DFT results (b). The experimental gas phase absorption spectrum of porphine [21] is drawn with a continuous line in both (a) and (b). The normalized absorbance is plotted as a function of absorption wavelength (nm). The values of the Q band absorbances have been multiplied by ten prior to normalization [21]. The MRMP [51], DFT-SCI [54], and TD-DFT [19,55,56] results taken from literature are presented schematically in boxes in (c).

absorption spectrum has been drawn with a continuous line by using the experimental data available in literature [70]. Normalized values of absorbance have been plotted as a function of wavelength. Also the calculated oscillator strengths have been normalized to one. The wavelengths corresponding to the electronic transitions computed by the MRMP [51] and TD-DFT/B3LYP/6-31G(d) [57] methods are also presented schematically in Fig. 4. Inspection of Fig. 4 reveals that each absorption peak of zinc porphine is generated by two overlapping one-electron transitions.

According to both our results and the results of recent TD-DFT calculations for other metalloporphyrins [71] the molecular orbitals with energies lower than the energy of HOMO − 1 are involved in one-electron transitions in the near UV region, see Fig. 4. Also in the case of zinc porphine there is a good correspondence between calculated and experimental excitations, although examination of Fig. 4 shows that the calculated excitations corresponding to the Q band are slightly shifted towards red. This can be regarded both as a missing influence of the solvent, which is present in the experimental spectrum, and in addition as an inherent problem of the PW91 functional, which produces a too low HOMO–LUMO gap. It is expected that the use of the B3LYP functional would increase the computed HOMO–LUMO gap, and therefore, the DFT calculated excitations corresponding to Q band would shift towards lower wavelengths leading to a better correlation between calculated and experimental wavelengths. The solvent effects will be studied in our future molecular dynamics work. As in the case of porphine, the oscillator strengths are not well reproduced by the DFT method.

3.3. Molecular structures of H_2P–O34 and ZnP–O34

The optimized structures of H_2P–O34 and ZnP–O34 are drawn in Figs. 5(a) and (b) and some bond lengths and bond angles are listed in Table 4. The complete sets of Cartesian coordinates are available on request. According to our knowledge, no experimental data is available in literature on the structural parameters presented in Table 4. The differences in magnitudes of the bond lengths and bond angles of the porphyrin ring in H_2P–O34 compared to porphine (see Table 1) are within 0.015 Å and 2.5°, respectively. In the case of ZnP–O34 the changes of the bond lengths of the porphyrin ring are within 0.5 Å and those of the bond angles within 2.0° when compared to zinc porphine. These changes are due to the effects of the substituents. Both the H_2P–O34 and ZnP–O34 molecules have four phenyl groups attached to the *meso*-carbon atoms of the porphyrin ring. Three of the phenyl rings have *tert*-butyl groups at both *meta*-positions and the fourth phenyl ring has only a 3,4-dimethylbentsamide group attached to the *ortho*-position.

Table 3
Calculated and experimental [21] wavelengths (nm), energies (eV), and oscillator strengths of the electronic transitions of porphine

DFT/PW91/DNP			TD- DFT/PBE/SVP			Experimental		
Wavelength (nm)	Energy (eV)	Oscillator strength	Wavelength (nm)	Energy (eV)	Oscillator strength	Wavelength (nm)	Energy (eV)	Oscillator strength
637.3	1.94	0.4112 and 0.4075	578.3	2.14	0.0019	627.0	1.98	0.02
566.8	2.18	0.5798 and 0.6293	543.7	2.28	0.0012	511.5	2.42	0.07
426.7	2.90	0.0997	420.1	2.95	0.0974	–	–	–
426.3	2.91	0.0773	415.4	2.98	0.0225	–	–	–
374.4	3.31	0.0019	381.9	3.25	0.0007	–	–	–
346.5	3.58	0.0814	361.8	3.43	0.8580	372.0	3.33	1.15
346.5	3.58	0.0497	355.4	3.49	0.7598	372.0	3.33	

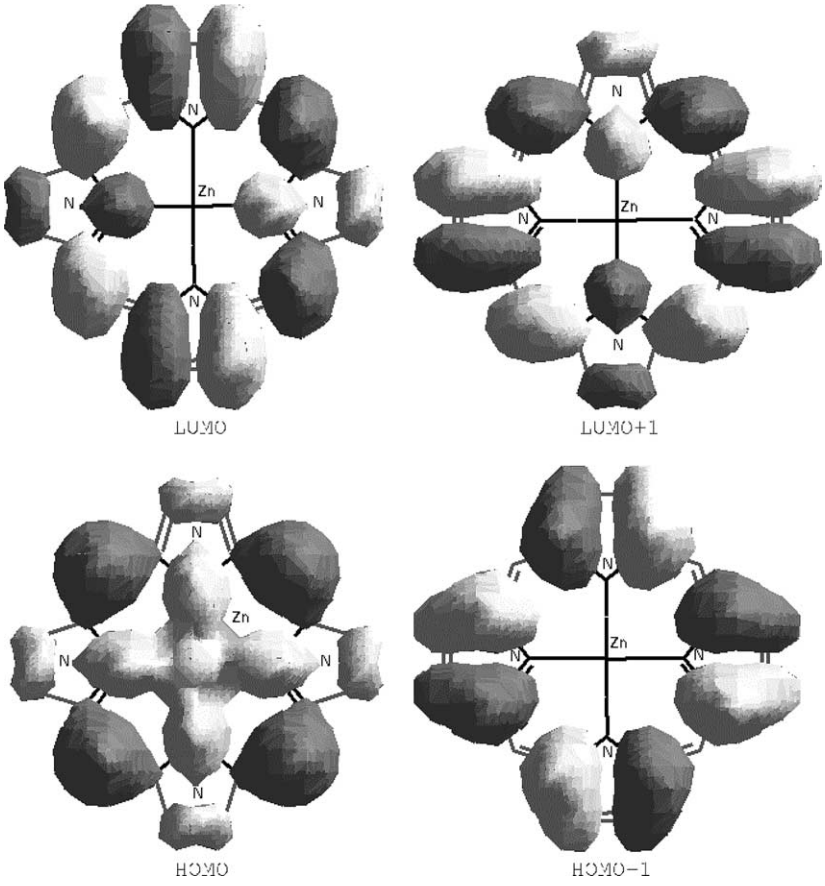

Fig. 3. Wavefunctions of some frontier molecular orbitals of the optimized molecular structure of zinc porphine are presented as isoamplitude surfaces. The sign of the wavefunction is indicated by light and dark regions.

Both molecules adopt a slightly non-planar geometry. The porphyrin ring has a ruffled [72] conformation in H_2P–O34 and a waved [72] conformation in ZnP–O34. Also, ongoing molecular dynamic calculations on the H_2P–O34–C_{60} dyad predict that the ruffled conformation of the porphyrin ring is the representative conformation. The dihedral angles between the phenyl substituents and the porphyrin ring in H_2P–O34 and ZnP–O34 are 63.4–70.3° and 62.4–68.9°, respectively. In TPP dihedral angles of >60° have been observed by X-ray crystallography [73]. The magnitudes of the dihedral angles influence the electronic interaction between all substituents and the porphyrin ring itself [5,7], as will be discussed below. Substituents do not only induce non-planarity and other structural changes but affect also the entire electronic structure of the original porphyrin ring.

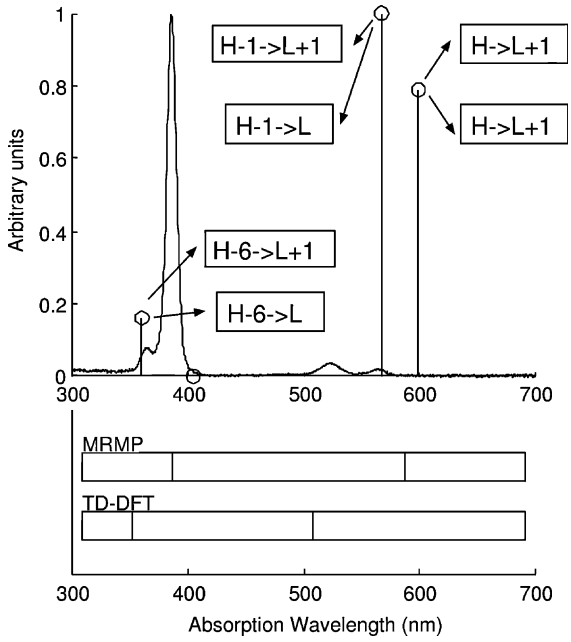

Fig. 4. Calculated DFT oscillator strengths and absorption wavelengths (nm) of one-electron transitions of zinc porphine are presented as separate bars in the upper graph. The initial and final orbitals involved in the one-electron transitions are also given in the upper figure. Only the one-electron transitions in the region of 350–700 nm have been considered. Experimental absorption spectrum of zinc porphine [70] is drawn with a continuous line. The MRMP [51] and TD-DFT/B3LYP/6-31G(d) [57] results presented schematically in boxes have been taken from literature.

3.4. Frontier molecular orbitals of H_2P–O34 and ZnP–O34

The energies of some FMOs of H_2P–O34 and ZnP–O34 are shown in Figs. 6 and 7, respectively. Different substituents, which have been added to the porphyrin ring of porphine and zinc porphine, induce variations on molecular orbital energies, see Figs. 6 and 7. The changes in energies of the LUMO, LUMO + 1, HOMO, and HOMO − 1 orbitals, which will be shown to be predominantly involved in the electronic transitions, are analyzed below. The wavefunctions of some frontier molecular orbitals of H_2P–O34 and ZnP–O34 are presented as isoamplitude surfaces in Figs. 8 and 9. Low-value isosurfaces are needed in order to reveal the amplitudes on the zinc atom in zinc porphyrins.

As in the case of porphine and zinc porphine, the LUMO and LUMO + 1 are almost degenerate, i.e., the energy difference is only 0.04 eV in H_2P–O34 and 0.03 eV in ZnP–O34. The energy differences between these molecular orbitals and the remaining unoccupied molecular orbitals are larger than 1 eV. In addition, the substituents raise the energies of both LUMO and LUMO + 1 of the H_2P–O34 and ZnP–O34 molecules by approximately the same amount (0.10–0.14 eV) from the corresponding energies of porphine and zinc porphine.

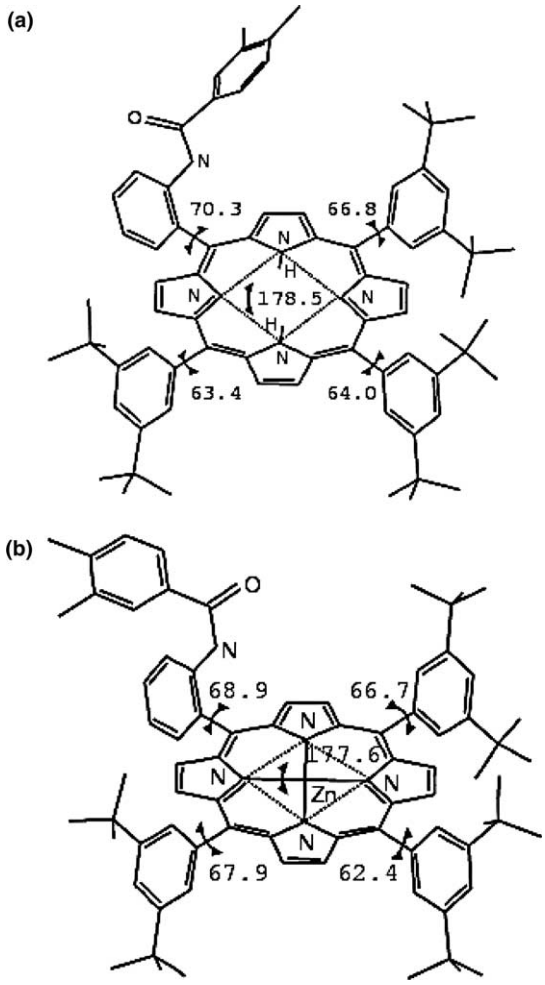

Fig. 5. Optimized molecular structures of (a) H_2P–O34 and (b) ZnP–O34. The hydrogen atoms have been omitted except from the nitrogen atoms of the pyrrole rings. The numbers in the figures represent the values of the dihedral angles, in degrees, between the phenyl rings and the porphyrin ring.

The energies of the HOMO and HOMO − 1 increase by at least twice as much (0.17–0.34 eV) whereas the energies of the HOMO orbitals increase more than the energies of the HOMO − 1 orbitals. Therefore, the HOMO–LUMO energy gap in H_2P–O34 and ZnP–O34 is smaller than in porphine or zinc porphine. However, the energy gaps are only 12% and 6% smaller, respectively, because both the LUMO and HOMO energies increase simultaneously.

The differences between the molecular orbital energies of H_2P–O34 and porphine or ZnP–O34 and zinc porphine can be attributed partially to the distortion of the porphyrin ring from a planar structure. The distortion is destabilizing the occupied FMOs and to a smaller extent the unoccupied FMOs. In addition, both the locations and the electronic properties of the substituents of the porphyrin ring determine the amount of changes in the molecular orbital energies. In order to quantify the contribution of the geometrical changes alone we

Table 4
Some calculated bond lengths (Å) and bond angles (°) in H_2P–O34 and ZnP–O34 molecules

H_2P–O34	Bond length (Å)	Bond angle (°)	ZnP–O34	Bond length (Å)	Bond angle (°)
H–N	1.026		Zn–N	2.059–2.060	
N–C_α	1.377–1.379		N–C_α	1.378–1.379	
(N–C_α)[a]	1.371–1.372		C_β–C_α	1.443–1.444	
C_β–C_α	1.432–1.434		C_β–C_β	1.365–1.357	
(C_β–C_α)[a]	1.457–1.458		C_m–C_α	1.412–1.413	
C_β–C_β	1.373–1.376		C_β–H	1.086–1.088	
(C_β–C_β)[a]	1.358–1.359				
C_m–C_α	1.407–1.409				
(C_m–C_α)[a]	1.414–1.415				
C_β–H	1.086–1.088				
(C_β–H)[a]	1.086–1.087				
α(H–N–C_α)		126.4–126.8	α(N–Zn–N)		89.8–90.1
α(C_α–N–C_α)		110.7–110.8	α(C_α–N–C_α)		106.9–107.0
α(C_α–N–C_α)[a]		105.4	α(N–C_α–C_β)		109.3–109.5
α(N–C_α–C_β)		106.4–106.5	α(C_α–C_β–C_β)		107.1–107.2
α(N–C_α–C_β)[a]		110.9	α(C_α–C_m–C_α)		124.9–125.0
α(C_α–C_β–C_β)		108.1–108.2	α(Zn–N–C_α)		125.9–126.0
α (C_α–C_β–C_β)[a]		106.3–106.5			
α(C_α–C_m–C_α)		125.0–125.7			

[a] Bonds and angles are in the pyrrole rings in which the nitrogen atoms are unprotonated.

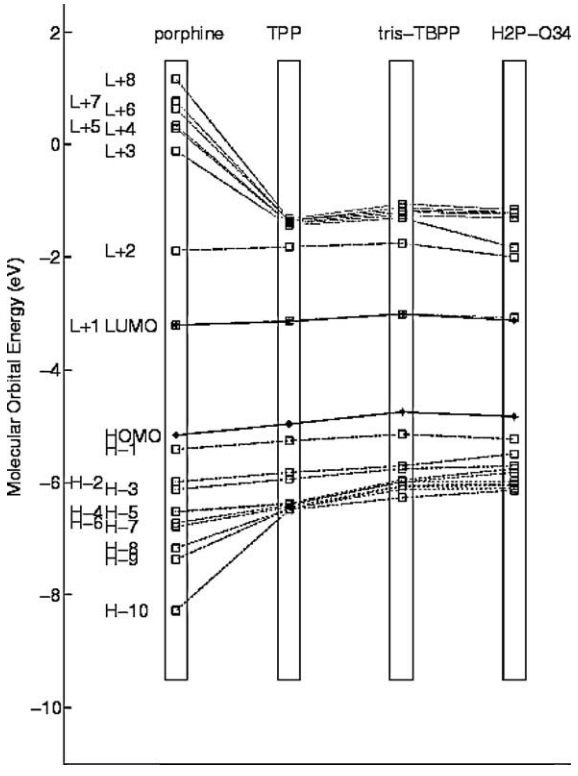

Fig. 6. Energies (eV) of some molecular frontier orbitals of porphine, TPP, tris-TBPP, and H_2P–O34. Solid lines are used for presenting the variations in energies of the HOMO and the LUMO, dashed lines for presenting the variations in energies of HOMO − 1 through HOMO- − 10, and dotted lines in the case of LUMO + 1 through LUMO + 8.

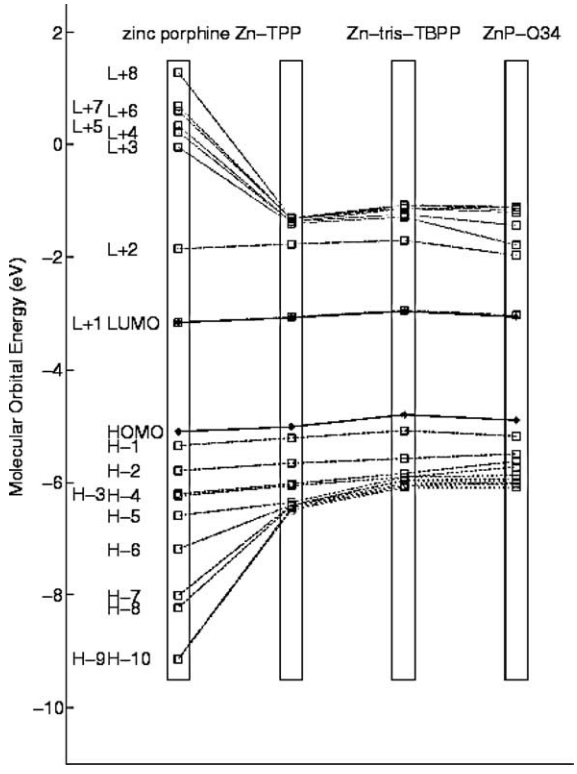

Fig. 7. Energies (eV) of some molecular frontier orbitals of zinc porphine, Zn–TPP, Zn–tris-TBPP, and ZnP–O34. Solid lines are used for presenting the variations in energies of the HOMO and the LUMO, dashed lines for presenting the variations in energies of HOMO − 1 through HOMO − 10, and dotted lines in the case of LUMO + 1 through LUMO + 8.

have carried out DFT/PW91/DNP calculations for modified H_2P–O34 (*m*-H_2P–O34) and ZnP–O34 (*m*-ZnP–O34) molecules in which all the substituents were replaced by hydrogens while retaining the distorted porphyrin skeleton [14]. The HOMO–LUMO gaps of (*a*) H_2P–O34 and ZnP–O34 are 1.71 and 1.84 eV, re-

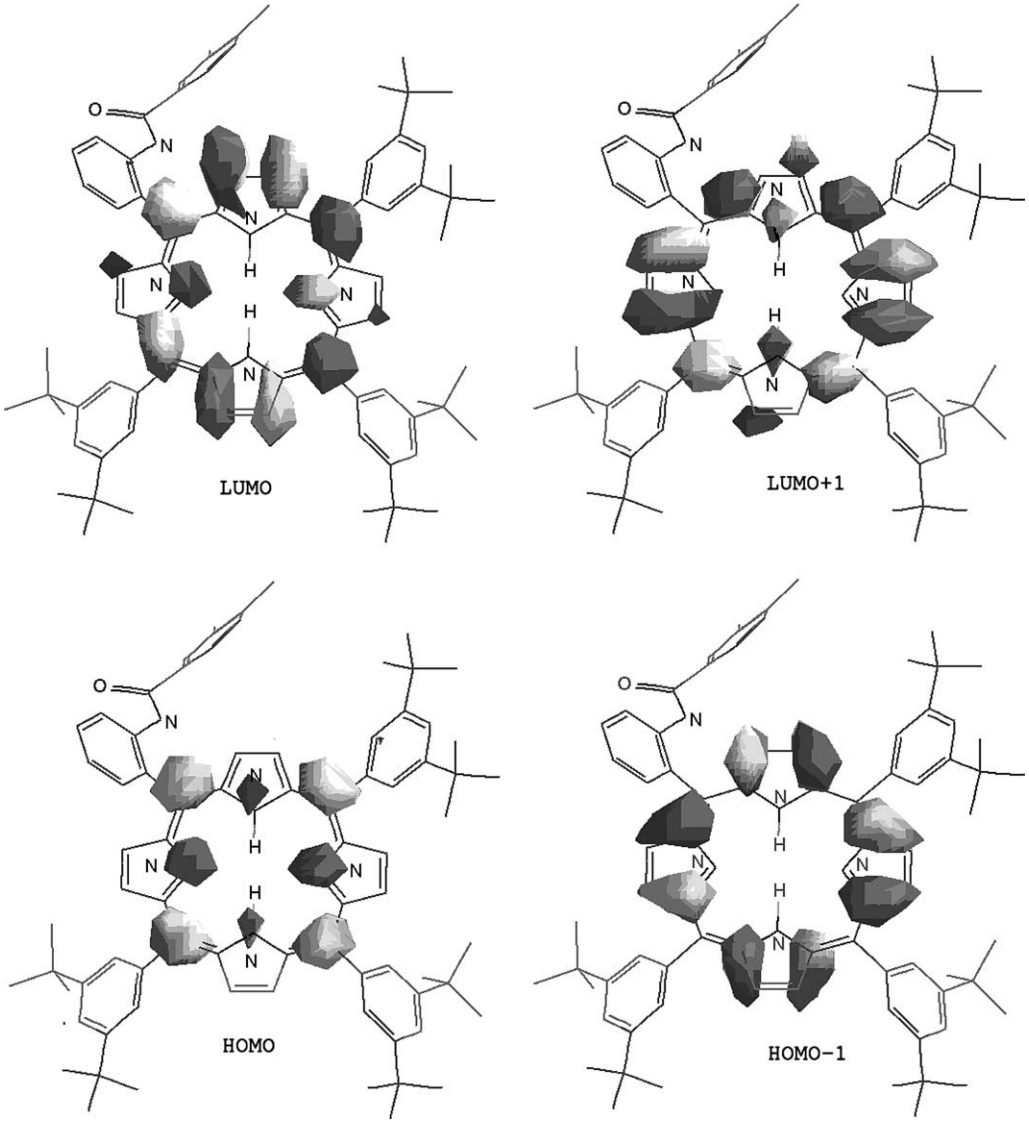

Fig. 8. Wavefunctions of some frontier molecular orbitals of H_2P–O34 presented as isoamplitude surfaces. The sign of the wavefunction is indicated by light and dark regions.

spectively. The HOMO–LUMO energy gaps of (*b*) *m*-H_2P–O34 and *m*-ZnP–O34 are 1.91 and 2.03 eV, respectively. The distortion of the geometry contributes <20% to the decrease of the HOMO–LUMO energy gap. The HOMO–LUMO energy gaps (*R*) of porphine (1.95 eV) and zinc porphine (2.07 eV) were taken as references, see Table 2 and Fig. 7. The contribution is $x = [(b - R)/(a - R)] \times 100\%$, which means that the decreases of the HOMO–LUMO energy gaps of the modified *m*-H_2P–O34 and *m*-ZnP–O34 with respect to the reference HOMO–LUMO energy gaps are divided by the decreases of the HOMO–LUMO energy gaps of H_2P–O34 and ZnP–O34 with respect to the reference and multiplied by 100%.

The influences which the locations of the substituents and their electronic properties have on the energies of the MOs can be determined by firstly inspecting the isoamplitude surfaces of HOMO − 1, HOMO, LUMO, and LUMO + 1 of zinc porphine, H_2P–O34, and ZnP–O34, see Figs. 3, 8 and 9. From Figs. 3, 8 and 9 it can be seen that the nodal patterns of isoamplitude surfaces of HOMO orbitals differ from those of the HOMO − 1 orbitals. Also the nodal patterns of the LUMO orbitals differ from those of the LUMO + 1 orbitals. In the case of *meso*-carbon and nitrogen atoms the amplitudes of the wavefunctions of the HOMO orbitals are high, whereas the HOMO − 1 orbitals have nodal planes. On the other hand, the amplitudes of the wavefunctions are low for the HOMO orbitals at α and β carbons and high for the HOMO − 1 orbitals. In addition, in the case of ZnP–O34 the wavefunction of the HOMO has non-zero amplitude on the zinc atom, whereas the amplitude of the HOMO − 1 wavefunction is zero. Also the other porphyrin molecules studied in this work, i.e., porphine,

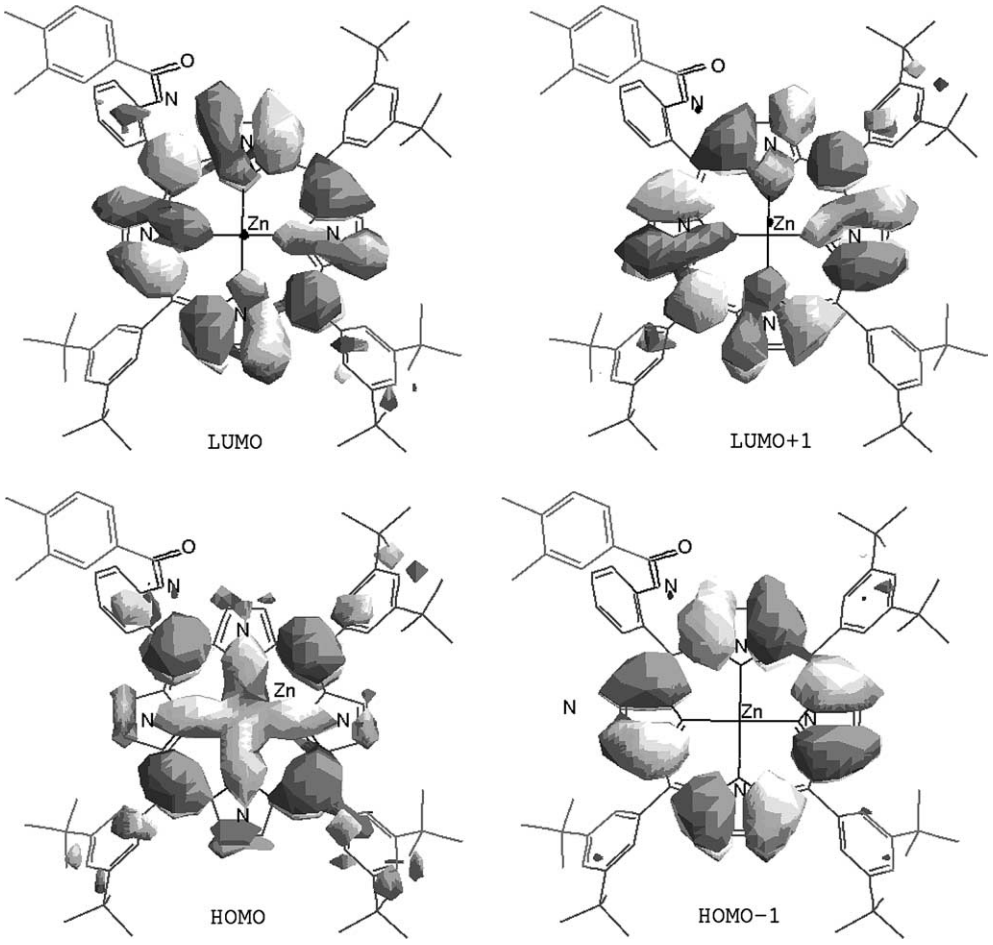

Fig. 9. Wavefunctions of some frontier molecular orbitals of ZnP–O34 presented as isoamplitude surfaces. The sign of the wavefunction is indicated by light and dark regions.

TPP, Zn–TPP, tris-TBPP, and Zn–tris-TBPP, exhibit the same characteristics in the amplitudes of their wavefunctions for HOMO − 1, HOMO, LUMO, and LUMO + 1. Therefore, electron donating and withdrawing substituents, which have been added to the *meso*-carbons, are able to change the energy of the HOMO of porphine and zinc porphine but do not significantly affect the energy of the HOMO − 1.

The increase in the energies of the HOMOs of H_2P–O34 and ZnP–O34 compared to porphine and zinc porphine is caused by the combined electronic effects of phenyl substituents and of substituents located at the phenyl rings. Each phenyl group has an electron donating inductive effect. The conjugation of the π electrons of phenyls with the π electrons of a porphyrin ring, which would lower the energy of the HOMO orbitals, is hindered by large dihedral angles between the planes of the phenyls and the prophyrin ring [5]. Therefore, these substituents increase the energies of the HOMOs of TPP and Zn–TPP compared to porphine and zinc porphine. The *tert*-butyl groups, which have an electron donating inductive effect, increase the energy of the HOMO of tris-TBPP and Zn–tris-TBPP in comparison to the HOMO of TPP and Zn–TPP. On the other hand, the addition of a benzamide group to the fourth phenyl group of tris-TBPP and Zn–tris-TBPP decreases the energy of the HOMO slightly. The benzamide group both withdraws electrons by a small inductive effect and also donates electrons by resonance. However, NMR studies [74] and other experimental studies [7] have shown that only the inductive electronic effects of substituents located at the *meta*-positions of the phenyl rings are felt strongly by the electrons of the porphyrin ring. Therefore, the energy of the HOMO is influenced by the electron withdrawing inductive effect and not by the resonance effect of the benzamide group.

3.5. Near UV–Vis optical absorption spectra

The DFT method has been used to calculate the wavelengths and the oscillator strengths of the one-electron transitions corresponding to the optical absorptions of H_2P–O34 and ZnP–O34. The experimental absorption spectra of H_2P–O34 and ZnP–O34 have been

measured in benzene by us using a Shimadzu UV-3100PC spectrophotometer with a 2 nm slit. The calculated oscillator strengths and the measured absorbances of H_2P–O34 and Zn–O34 were plotted as a function of wavelength and are illustrated in Figs. 10(a) and (b). The maximum values of the oscillator strengths and absorbances have been normalized to one.

Based on the calculations performed on porphine and zinc porphine, we expect that the following qualitative and quantitative conclusions can be drawn from the DFT calculations on H_2P–O34 and ZnP–O34. The B band in H_2P–O34 and ZnP–O34 is generated by several one-electron transitions to the LUMO and LUMO + 1 orbitals. Experimental results of fluorescence spectroscopy measurements of porphyrins indicate that the excited state, that corresponds to the B band absorption, should be described as a manifold of vibronic levels belonging to two or more electronic states [75]. Also orbitals with energies lower than the energy of HOMO and HOMO − 1 are involved in the one-electron transitions taking place in the near UV region. The number of one-electron transitions giving rise to the B band is much larger in H_2P–O34 and ZnP–O34 than in the unsubstituted porphyrins. The high number is due to the complexities of the electronic structures and low symmetries (C_1) of these molecules. The Q_x^0 and Q_y^0 peaks are generated by one-electron transitions involving predominantly the HOMO − 1, HOMO, LUMO, and LUMO + 1 orbitals. Examination of Fig. 10 reveals that the same problems discussed above for porphine and zinc porphine which are related to (a) the failure to correctly evaluate the oscillator strengths and to (b) the red shifts of the calculated excitations with respect to the experimental peaks of the Q band can be also observed for the DFT results of H_2P–O34 and ZnP–O34.

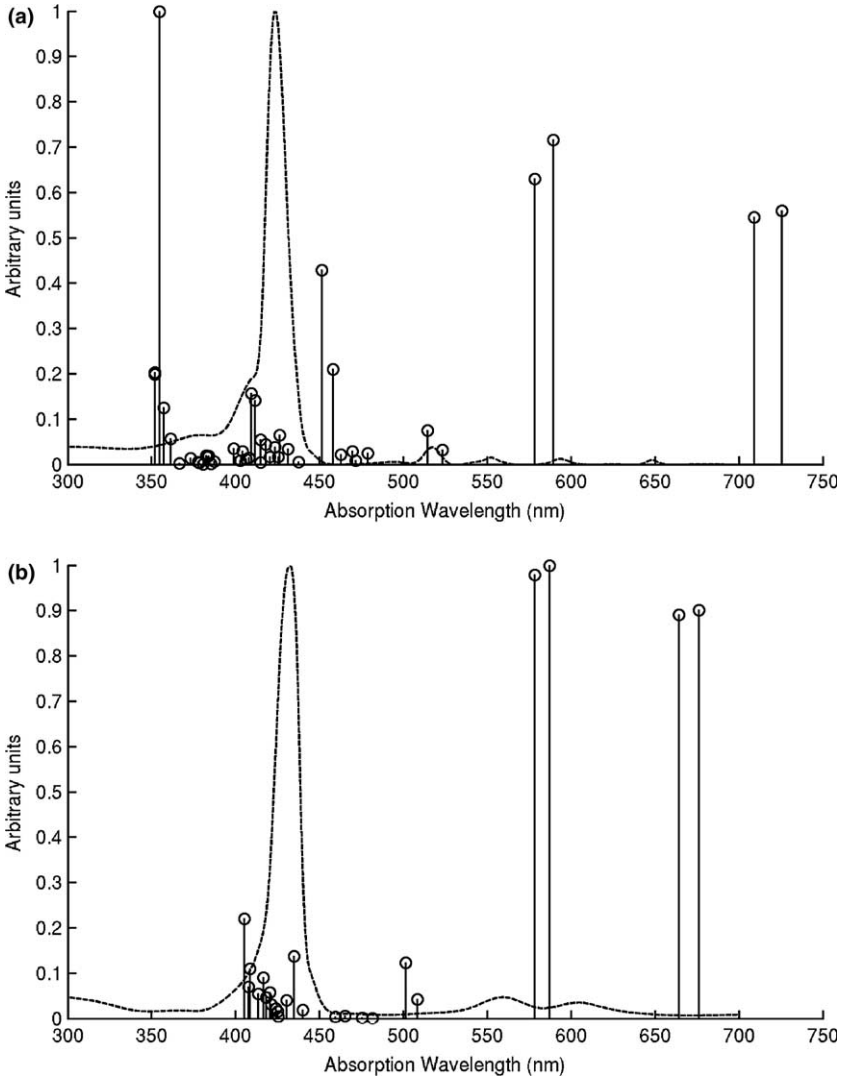

Fig. 10. Calculated DFT one-electron transitions and measured absorption spectra of (a) H_2P–O34 and (b) ZnP–O34. Only the electronic transitions corresponding to the absorptions in the region of 350–750 nm have been considered.

Inspection of the calculated electronic transitions shown in Figs. 2(a), 4 and 10 reveals that our calculations predict red shifts of the absorption maxima of H_2P–O34 and ZnP–PO34 as compared to porphine and zinc porphine, respectively. Red shifts are also observed when the experimental spectrum of porphine in benzene [21], Fig. 2(a), is compared with the spectrum of H_2P–O34 in benzene, Fig. 10(a). The maxima of the experimental Q_x^0 and Q_y^0 peaks and of the B band are located at 617.3, 520.8 and 396.5 nm in the case of porphine [21] and at 648.0, 552.0 and 423.0 nm in the case of H_2P–O34, Fig. 10(a), respectively. Inspection of the experimental spectra of ZnP–O34, Fig. 10(b), and zinc porphine, Fig. 4, reveals that all absorption maxima of the substituted zinc porphine also shift to red with respect to the unsubstituted zinc porphine. The red shifts are due to the electronic effects of the substituents as well as to the non-planarity caused by the substituents. On the basis of the influence that the distortion of the porphyrin ring has on the HOMO–LUMO gap, the contribution of the distortion to the red shifts is expected to be less than 20%. Therefore, although the contribution of the electronic effects of the substituents to the observed red shifts can be evaluated to be as high as 80%, a more detailed analysis based on TD-DFT calculations is needed. The TD-DFT method has been proven to be successful in predicting and analyzing the origin of the spectral shifts of porphyrin molecules [15,19,20]. We will apply also the TD-DFT method to H_2P–O34 and ZnP–O34 in the future and report the results in the next paper.

4. Conclusions

Our DFT and TD DFT results show that the ground state based DFT method for calculating the electronic transitions allows a reliable and rapid evaluation of energies and orbitals involved in one-electron transitions in porphyrin molecules but fails in evaluating the oscillator strengths associated with transitions. Moreover, this method gives a clear picture of the electron transfer processes by restricting the calculations to the well-defined final states of the transitions. It is expected to yield insight into the electron transfer paths in porphyrin–fullerene dyads, which we will mainly concentrate in our future work. However, it is not meant for the calculations of the excitation spectra, in which case methods like TD-DFT, MRMP, and SAC-CI can be applied more reliably.

In this work, the DFT method was used to calculate the ground state geometries, electronic structures, and one-electron transitions of two asymmetrically substituted porphyrin molecules, i.e., H_2P–O34 and ZnP–O34. It is assumed that this method calculates the geometries of H_2P–O34 and ZnP–O34 as accurately as that of porphine, because there are no experimental bond lengths and bond angles available for H_2P–O34 and ZnP–O34 for comparison.

In order to evaluate the influence of the substituents on the ground state geometries and the electronic structures also the symmetric unsubstituted porphyrins, i.e., porphine and zinc porphine as well as the partially substituted porphyrins, i.e., TPP, *tris*-TBPP, and their zinc complexes, together with the modified *m*-H_2P–O34 and *m*-ZnP–O34 structures were investigated using the same method. The method used in this work describes correctly the differences in electronic structures and in the HOMO–LUMO gaps of the porphyrin molecules, which have different substituents. It was shown that the distortions induced by the substituents to the porphyrin ring contribute less than 20% to the changes of the HOMO–LUMO gap energies of H_2P–O34 and ZnP–O34 when compared to porphine and zinc porphine.

The electronic effects of the substituents influence the HOMO energies more than the HOMO − 1 energies because HOMOs have high amplitudes at the *meso*-carbons, to which the substituents are bonded, whereas HOMO − 1 orbitals have nodal planes through the *meso*-carbons. The HOMO energies of TPP and Zn–TPP increase if compared to porphine and zinc porphine, because the phenyl groups donate electrons inductively. The HOMO energies of tris-TBPP and tris-Zn-TBPP increase if compared to TPP and Zn–TPP because the *tert*-butyl groups donate electrons inductively. The HOMO energies of H_2P–O34 and ZnP–O34 decrease if compared to tris-TBPP and tris-Zn-TBPP because the benzamide group withdraws electrons from the porphyrin ring inductively. The donation of electrons from the benzamide group by resonance is hindered because of the hindered π conjugation.

The calculated energies (wavelengths) of the electronic transitions, which give rise to the Q and B bands, compare well with the energies (wavelengths) of the experimentally determined absorption maxima. The ground based state DFT method predicts correctly also the experimentally observed red shifts of the absorption wavelengths of the substituted porphyrins with respect to the unsubstituted porphyrins. The red shifts are due to the locations and electronic effects of the substituents.

Acknowledgements

The authors acknowledge the financial support from the ''National Graduate School in Materials Physics'', financed by the Academy of Finland, and the computing resources provided by the Finnish IT center for Science (CSC), Espoo, Finland. Professor Helge Lemmetyinen and the experimental research group at the Institute of Materials Chemistry, Tampere University of Technol-

ogy, Finland, are acknowledged for pointing out the experimental data and extensive discussions related to porphyrin based dyads and photoinduced electron transfer within these types of molecules. The authors thank Professor Hiroshi Imahori from Japan and his research group for their collaboration with the experimental group of our laboratory.

References

[1] H. Imahori, K. Hagiwara, M. Aoki, T. Akiyama, S. Taniguchi, T. Okada, M. Shirakawa, Y. Sakata, J. Am. Chem. Soc. 118 (1996) 11771.
[2] V. Vehmanen, V.N. Tkachenko, H. Imahori, S. Fukuzumi, H. Lemmetyinen, Spectrochim. Acta A 57 (2001) 2229.
[3] H. Imahori, V.N. Tkachenko, V. Vehmanen, K. Tamaki, H. Lemmetyinen, Y. Sakata, S. Fukuzumi, J. Phys. Chem. A 105 (2001) 1750.
[4] M. Nappa, J.S. Valentine, J. Am. Chem. Soc. 100 (1978) 5075.
[5] S.K. Suslick, C. Chen, R.G. Meredith, L. Cheng, J. Am. Chem. Soc. 114 (1992) 6928.
[6] G.P. Gassman, A. Ghosh, J. Almlöf, J. Am. Chem. Soc. 114 (1992) 9990.
[7] R. Koerner, J.L. Wright, X.D. Ding, M.J.M. Nesset, K. Aubrecht, R.A. Watson, R.A. Barber, L.M. Mink, A.R. Tipton, C.J. Norvell, K. Skidmore, U. Simonis, F.A. Walker, Inorg. Chem. 37 (1998) 733.
[8] J.D. Spence, T.D. Lash, J. Org. Chem. 65 (2000) 1530.
[9] N.E. Gruhn, D.L. Lichtenberger, H. Ogura, F.A. Walker, Inorg. Chem. 38 (1999) 4023.
[10] M.K. Karl, M.S. Kevin, R. Guilard, in: The Porphyrin Handbook, vol. 8, Academic Press, New York, 2000.
[11] M. Gouterman, J. Chem. Phys. 30 (1959) 1139.
[12] A. Ghosh, Acc. Chem. Res. 31 (1998) 189.
[13] T. Vangberg, A. Ghosh, J. Am. Chem. Soc. 120 (1998) 6227.
[14] A.K. Nguyen, N.P. Day, R. Pachter, J. Phys. Chem. A 103 (1999) 9378.
[15] K.A. Wertsching, S.A. Koch, S.G. DiMagno, J. Am. Chem. Soc. 123 (2001) 3932.
[16] R.E. Haddad, S. Gazeau, J. Pecaut, J.-C. Marchon, C.J. Medforth, J.A. Shelnutt, J. Am. Chem. Soc. 125 (2003) 1253.
[17] I.H. Wasbotten, J. Conradie, A. Ghosh, J. Phys. Chem. B 107 (2003) 3613.
[18] M.K. Karl, M.S. Kevin, R. Guilard, in: The Porphyrin Handbook, vol. 7, Academic Press, New York, 2000.
[19] K.A. Nguyen, P.N. Day, R. Pachter, J. Phys. Chem. A 104 (2000) 4748.
[20] K.A. Nguyen, P.N. Day, R. Pachter, J. Phys. Chem. A 106 (2002) 10285.
[21] L. Edwards, D.H. Dolphin, M. Gouterman, A.D. Adler, J. Mol. Spectrosc. 38 (1971) 16.
[22] B.F. Kim, J. Bohandy, J. Mol. Spectrosc. 73 (1978) 332.
[23] J. Dalton, L.R. Milgrom, S.M. Permberton, J. Chem. Soc., Perkin Trans. 2 (1980) 370.
[24] M. Gouterman, J. Mol. Spectrosc. 6 (1961) 138.
[25] M. Gouterman, G.H. Wagniére, J. Mol. Spectrosc. 11 (1963) 108.
[26] W. Koch, M.C. Holthausen, A Chemist's Guide to Density Functional Theory, second ed., Wiley VCH, New York, 2001.
[27] J.M. Seminario, Recent Developments and Applications of Modern Density Functional Theory, Elsevier, Amsterdam, 1996.
[28] R.G. Parr, W. Yang, Density Functional Theory of Atoms and Molecules, Oxford University Press, Oxford, 1994.
[29] M. Sieger, M. Wanner, W. Kaim, J.S. Derk, L.S. Theo, S. Zális, Inorg. Chem. 42 (2003) 3340.
[30] K. Zheng, X. Liu, D. Hong, C. Hui, F. Yun, L. Ji, THEOCHEM 626 (2003) 295.
[31] R. Hermann, S. Naumov, O. Brede, THEOCHEM 532 (2000) 69.
[32] L.C. Bo, C.P. Cheu, P.M.L. Zhi, J. Phys. Chem. A 107 (2003) 5241.
[33] C. Dutan, S. Choua, T. Berclaz, M. Geoffry, N. Mézailles, A. Moores, L. Richard, P. Le Floch, J. Am. Chem. Soc. 125 (2003) 4487.
[34] J.-P. Blaudeau, D.S. Dudis, A.T. Yeates, T.M. Cooper, 226th ACS National Meeting, 2003.
[35] K. Wissing, J.A. Aramburu, M.T. Barriuso, M. Moreno, Radiat. Effects Defects Solids 151 (1999) 1.
[36] A.A. Valladares, R.M. Valladares, A. Valladares, M.A. Mc Nelis, Synth. Met. 103 (1999) 2570.
[37] R.M. Valladares, A.G. Calles, A.A. Valladares, Synth. Met. 103 (1999) 2572.
[38] H. Jiang, R. Pandey, C. Darrigan, M. Rérat, J. Phys. Condens. Matter 15 (2003) 709.
[39] P. Boulet, M. Buchs, H. Chermette, C. Daul, E. Furet, F. Gilardoni, F. Rogemond, C.W. Schläpfer, J. Weber, J. Phys. Chem. 105 (2001) 8999.
[40] H. Pinto, S. Elliott, A. Stashans, Proc. SPIE-Int. Soc. Opt. Eng. 5122 (2003) 303.
[41] A.J. Williamson, J.C. Grossman, R.Q. Hood, A. Puzder, G. Galli, Phys. Rev. Lett. 89 (2002) 196803-1.
[42] M. Palummo, G. Onida, R. Del Sole, B.S. Mendoza, Phys. Rev. B 60 (1999) 2522.
[43] J. von Knop, A. Knop, Z. Naturforsch. A 25 (1970) 1720.
[44] M.G. Maggiora, L. Weimann, J. Chem. Phys. Lett. 22 (1973) 297.
[45] N. Matsuzawa, M. Ata, D.A. Dixon, J. Phys. Chem. 99 (1995) 7698.
[46] J. Almlöf, T.H. Fischer, P.G. Gassman, A. Ghosh, M. Haser, J. Phys. Chem. 97 (1993) 10964.
[47] M. Merchán, E. Ortí, O.R. Björn, Chem. Phys. Lett. 221 (1994) 136.
[48] D. Lamoen, M. Parinello, Chem. Phys. Lett. 248 (1996) 309.
[49] H. Nakatsuji, J. Hasegawa, M. Hada, J. Chem. Phys. 104 (1996) 2321.
[50] Y. Tokita, J. Hasegawa, H. Nakatsuji, J. Phys. Chem. A 102 (1998) 1843.
[51] T. Hashimoto, Y. Choe, H. Nakano, K. Hirao, J. Phys. Chem. A 103 (1999) 1894.
[52] A.K. Nguyen, R. Pachter, in: Tech. Proc. 1999 Int. Conf. MSM, 1999, p. 57.
[53] M. Tazi, P. Lagant, G. Vergoten, J. Phys. Chem. A 104 (2000) 618.
[54] A.B.J. Parusel, A. Ghosh, J. Phys. Chem. A 104 (2000) 2504.
[55] S.J.A. van Gisberg, A. Rosa, G. Ricciardi, E.J. Baerends, J. Chem. Phys. 111 (1999) 2499.
[56] D. Sundholm, Phys. Chem. Chem. Phys. 2 (2000) 2275.
[57] K.A. Nguyen, R. Pachter, J. Chem. Phys. 114 (2001) 10757.
[58] Dmol User Guide, October 1995, San Diego: MSI, 1995.
[59] J.P. Perdew, J.A. Chevary, S.H. Vosko, K.A. Jackson, M.R. Pederson, D.J. Singh, C. Fiolhais, Phys. Rev. B 46 (1992) 6671.
[60] P.W. Atkins, R.S. Friedman, Molecular Quantum Mechanics, Oxford University Press, Oxford, 1997.
[61] R. Ahlrichs, M. Bär, M. Häser, H. Horn, C. Kälmel, Chem. Phys. Lett. 162 (1989) 165.
[62] P.J. Perdew, K. Burke, M. Ernzerhof, Phys. Rev. Lett. 77 (1996) 3865.
[63] J.C. Slater, Phys. Rev. 81 (1951) 385.
[64] P.A.M. Dirac, Proc. R. Soc. 123 (1929) 714.
[65] M. Swart, J.G. Snijders, Theor. Chem. Acc. 110 (2003) 34.
[66] J.P. Perdew, K. Burke, Y. Wang, Phys. Rev. B 54 (1996) 16533.
[67] A. Schäfer, H. Horn, R. Ahlrichs, J. Chem. Phys. 97 (1992) 2571.

[68] T.H. Dunning Jr., J. Chem. Phys. 90 (1989) 1007.
[69] K. Eichkorn, O. Treutler, H. Öhm, M. Häser, R. Ahlrichs, Chem. Phys. Lett. 240 (1995) 283.
[70] G.W. Canters, G. Jansen, M. Noort, J.H. vander Waals, J. Phys. Chem. 80 (1971) 2253.
[71] D. Sundholm, Chem. Phys. Lett. 317 (2000) 392.
[72] W.R. Scheidt, Y. Lee, J. Struct. Bonding (Berlin) 64 (1987) 1.
[73] S.J. Silvers, A. Tulinsky, J. Am. Chem. Soc. 89 (1967) 3331.
[74] F.A. Walker, V.L. Balke, G.A. McDermott, Inorg. Chem. 21 (1982) 3342.
[75] G.G. Gurzadyan, T.-H. Tran-Thi, T. Gustavsson, J. Chem. Phys. 108 (1998) 385.
[76] K.N. Solovyov, L.L. Gladkov, A.T. Gradyushko, N.M. Ksenofontova, A.S. Starukhin, J. Mol. Struct. 45 (1978) 267.